Quaternary Research

doi:10.1017/qua.2020.118

Causes and climatic influence of centennial-scale denitrification variability in the southeastern Arabian Sea since the last glacial period

Sidhesh Nagoji[a], Manish Tiwari[a]*

[a]National Centre for Polar and Ocean Research, Ministry of Earth Sciences, Vasco-da-Gama, Goa 403804, India
*Corresponding author e-mail address: manish@ncpor.res.in (M. Tiwari)

(Received June 8, 2020; Accepted November 16, 2020)

Abstract

Denitrification occurring in the oxygen minimum zone of the Arabian Sea produces nitrous oxide, a powerful greenhouse gas. Therefore, it is important to understand the mechanisms controlling denitrification's intensity and evaluate its influence on the global climate at various timescales. We studied multiple geochemical and isotopic proxies in a sediment core from the southeastern Arabian Sea (SEAS) at a high (centennial-scale) resolution. We find that since the last glacial period, both the ventilation and the productivity caused by the South Asian summer monsoon played a major role in controlling the denitrification variability in SEAS. During the Last Glacial Maximum (LGM) and since the Holocene, denitrification increased in SEAS despite reduced monsoon-induced productivity. During the LGM, weakened thermohaline circulation resulted in reduced ventilation of the intermediate waters of SEAS, causing increased denitrification. During the Holocene, the increase in denitrification is caused by an enhanced inflow of oxygen-depleted Red Sea and Persian Gulf waters into the intermediate depth of SEAS owing to a rising sea level that prohibited ventilation by the Antarctic Intermediate Water. We further find millennial-scale synchronicity between denitrification in SEAS, global monsoons, and the North Atlantic climate, implying systematic linkages via greenhouse gases abundance.

Keywords: Quaternary; Paleoceanography; Paleoclimatology; Global; Stable Isotopes; Monsoon; Denitrification; Arabian Sea; Teleconnection; Ventilation

INTRODUCTION

A previously long-held hypothesis that the North Atlantic is the driver of the tropical climate argues that climate perturbations originate in the high-latitude North Atlantic and propagate globally via various ocean-atmospheric pathways (e.g., Broecker et al., 1985; Goswami et al., 2006). Another hypothesis posits natural greenhouse gas concentrations modulated by climate conditions in the tropics, including monsoonal convection, as the principal factor governing the millennial-scale global climate change. Possibly, during warmer periods, excess moisture and greenhouse gases from the tropics acted as a positive feedback mechanism (e.g., Schulz et al., 1998; Kudrass et al., 2001; Ivanochko et al., 2005; Tiwari et al., 2006 and references therein). One such process that can influence greenhouse gases concentration is marine denitrification. This occurs in the oxygen minimum zones (OMZs) of the world's oceans and is an important component of the nitrogen cycle. Denitrification not only governs the bioavailable nitrogen required for oceanic productivity that sequesters atmospheric CO_2 but also produces nitrous oxide (N_2O), which is a powerful greenhouse gas.

OMZs are subsurface layers where oxygen concentration is less than 20 μmol L^{-1} and are observed between depths of 200 and 1200 m (Paulmier and Ruiz-Pino, 2009). They are found in regions where intense biological uptake of oxygen due to bacterial respiration and remineralization occurs and are associated with low oxygen supply via oceanic circulation. The present global warming may cause expansion and strengthening of the OMZs, which will have adverse consequences for marine flora and fauna and may provide positive feedback via N_2O emission through denitrification (Naqvi et al., 2000; Banse et al., 2014).

Denitrification occurs when the oxygen concentration in the OMZ falls below a threshold value of ~5 μmol/kg (Codispoti et al., 2001). During this process, nitrate (NO_3^-) acts as an

Cite this article: Nagoji, S., Tiwari, M. 2021. Causes and climatic influence of centennial-scale denitrification variability in the southeastern Arabian Sea since the last glacial period. *Quaternary Research* 101, 156–168. https://doi.org/10.1017/qua.2020.118

oxidizing agent and is finally reduced to dinitrogen (N_2) gas. In oceans, denitrification occurs in organic-rich continental margin sediments and subsurface water depths within intense OMZs (200–1200 m). Of the latter, the Arabian Sea supports approximately one-third of marine water column denitrification (Howell et al., 1997). During this process, bacteria preferentially consume NO_3^- with a lighter isotope (^{14}N) and thus enrich the residual NO_3^- in the heavier isotope (^{15}N) (Brandes and Devol, 2002). The ^{15}N-enriched NO_3^- is transported to the surface and consumed by phytoplankton, which subsequently settle down and get preserved in the sediments. Accordingly, the $\delta^{15}N$ of sedimentary organic matter (SOM) has been widely used as a tool to track changes in water column denitrification in this region (Altabet et al., 1995; Ganeshram et al., 1995, 2000 and references therein).

Previous research in the Arabian Sea observed strong denitrification and OMZ intensity during warm periods in the Northern Hemisphere (e.g., Dansgaard-Oeschger interstadials) and weak (or absent) intensity during cold periods (e.g., Heinrich events, Younger Dryas) (e.g. Schulz et al., 1998; Altabet et al., 2002; Singh et al., 2011). However, most of the previous studies on denitrification intensity from the southeastern Arabian Sea (SEAS) show low temporal resolution. Further, past denitrification intensity is used to infer past monsoon strength on millennial and longer timescales (e.g., Tiwari et al., 2010; Kessarkar et al., 2013). Consequently, higher-resolution past denitrification records from this region are needed to allow for a more detailed evaluation of the governing factors and influence of denitrification.

This study is one of the many studies we are carrying out in the eastern Arabian Sea to better understand the denitrification variability on million (Tripathi et al., 2017), multimillennial (Tripathi et al., 2020), and centennial (present study) timescales. We are also analyzing high-resolution denitrification data from another core (SK274-1G) from near the southern tip of India. The purpose is to explore the influence of denitrification on the global nitrogen and carbon cycles by including studies from the three major regions experiencing perennial pelagic denitrification: the eastern tropical South Pacific, the eastern tropical North Pacific, and the Arabian Sea. It may seem feasible to merge the data of the present study (core SK274-4G) with core SK274-1 G but doing so did not yield a cohesive picture, as the cores are from different locations and resolutions and have experienced dissimilar oceanographic processes. Moreover, the respective focus of the studies of the two cores is also different; merging them resulted in drastically reducing their scopes, especially of core SK274-1G, which will only be further explored once the findings from core SK274-4 G are published. The present study attempts to understand the underlying mechanisms governing the temporal variability of denitrification in SEAS at a high (centennial-scale) resolution since the last glacial period and its influence on the high-latitude climate using sediment core SK274-4 G from the continental slope of SEAS.

MODERN OCEANIC CONDITIONS IN THE EASTERN ARABIAN SEA

The Arabian Sea is characterized by a seasonal reversal of monsoon winds. Seasonal change in monsoon circulation drives significant changes in oxygen-deficient waters (Naqvi and Noronha, 1991) and surface water productivity (Bhattathiri et al., 1996; Madhupratap et al., 1996). During the South Asian summer monsoon (SASM), the circulation is along the eastern boundary: a West Indian coastal current (WICC) flows toward the equator, a northward undercurrent carries well-oxygenated waters off the Indian margin, and moderate coastal upwelling occurs. As the monsoon winds reverse during the winter season, the WICC flows northward, causing downwelling off the west coast of India and a relatively less oxygenated water column over the shelf. Therefore, the renewal of the oxygen-deficient subsurface waters is stronger during the SASM than during the winter monsoon.

The spatial variability of upwelling along the western continental margin of India can be inferred from water column productivity. During the pre-summer monsoon season, the sea surface temperature in the eastern Arabian Sea rises, thereby developing a mini warm pool, which then dissipates prior to the onset of summer monsoon precipitation as a result of upwelling (Shenoi et al., 1999). During the summer monsoon season, moderate to intense upwelling occurs as a result of the complex interaction between alongshore wind stress, coastally trapped Kelvin waves, and the offshore propagating Rossby waves (Lévy et al., 2007). This upwelling causes a several-fold increase in productivity (Lévy et al., 2007). Maximum chlorophyll (up to 7.8 µg/l) are observed in the northern part of the eastern Arabian Sea at this time (Banse, 1987), whereas during the winter monsoon season, northeast winds are too weak to induce any significant offshore Ekman transport in this region (Fontugne and Duplessy, 1986, Madhupratap et al., 1996). The perennial OMZ in the eastern Arabian Sea is observed at depths of between ~150 and 1200 m (Naqvi and Noronha, 1991). An oxygen-deficient condition in the intermediate depth develops because of high surface water productivity and sluggish ventilation, which results in denitrification (Naqvi and Noronha, 1991; Naqvi, 1994).

THE $\delta^{15}N$ OF THE ORGANIC MATTER IN THE EASTERN ARABIAN SEA

The marine nitrogen cycle is a complex phenomenon involving several processes, such as nitrogen fixation (N-fixation), NO_3^- utilization, denitrification, and anammox (anaerobic ammonium oxidation), through biologically mediated reactions. The nitrogen isotopes get mostly kinetically fractionated during these various steps, and it is therefore necessary to evaluate the conditions in the eastern Arabian Sea for correctly identifying the predominant process governing the $\delta^{15}N$ values of organic matter. Supplementary Figures 1a–d show the north–south transect of dissolved oxygen, NO_3^-, and nitrate deficit (N*) for the upper 2000 m (and upper 300 m for N*) in the Arabian Sea. N* is a tracer indicating

https://doi.org/10.1017/qua.2020.118 Published online by Cambridge University Press

deviations of the ratio of nitrogen to phosphorous from the 16:1 stoichiometric relationship (Gruber and Sarmiento, 2002). In the case of normal biological reactions, where the N:P ratio stays at 16:1, N* is a conservative property. But processes that use N:P in a ratio less (more) than 16:1 results in low (high) N* anomalies (Gruber and Sarmiento, 2002). Denitrification and N-fixation are such processes that result in low and high N* anomalies, respectively. N* can therefore be an important tool in identifying regions of denitrification and N-fixation.

N-fixation introduces new bioavailable nitrogen with low $\delta^{15}N$ values (Capone et al., 1998) into the ocean, thus compensating for the loss of NO_3^- during denitrification. The isotope effect during this process is very small ($\varepsilon = 0.2–3‰$), and the average $\delta^{15}N$ value of the resulting particulate organic nitrogen (PON) is -1‰. The N* variability in the near-surface water (Supplementary Fig. 1c) shows that N* exhibits low values, indicating very little N-fixation. Nevertheless, there is a slight addition of bioavailable nitrogen from north to south, as exhibited by a slight increase in N* values. This implies that the N-fixation is weak in the regions of strong denitrification. It agrees with the findings of Altabet et al. (1999) and Ganeshram et al. (2000) that the rate of N-fixation is too weak to significantly affect the $\delta^{15}N$ of NO_3^- in highly productive denitrification zones.

The incomplete utilization of NO_3^- by phytoplankton is a part of the internal cycling of nitrogen that leads to a small fractionation (isotope effect, $\varepsilon = \sim 0.2–3.0‰$), resulting in a slight increase in the $\delta^{15}N$ values (Sigman et al., 1997). It usually occurs where iron is the limiting factor that reduces the uptake of NO_3^- and thereby affects the $\delta^{15}N$ of the ambient waters (Ganeshram et al., 2000). In the Arabian Sea, NO_3^- is the limiting nutrient and is completely utilized in the near-surface photic zone (Supplementary Fig. 1b), so incomplete NO_3^- uptake does not affect the $\delta^{15}N$ values (Schafer and Ittekkot, 1993). Further, nitrogen assimilation in the form of nitrite (NO_2^-), NO_3^-, ammonium (NH_4^+), and urea results in isotope effects of ~1‰, ~5‰, ≤20‰, and ~1‰, respectively (Waser et al., 1998). These forms of nitrogen are almost completely consumed in the near-surface water and therefore produce minimal isotopic fractionation.

NO_3^- is removed via denitrification in oxygen-deficient zones. The largest isotopic fractionation (isotope effect, $\varepsilon = \sim 30‰$) takes place during denitrification in the water column (Sigman et al., 2009). The oceanic average $\delta^{15}N$ value of NO_3^- is ~5‰, and after experiencing denitrification, it increases to 15‰ or higher (Brandes et al., 1998; Rafter et al., 2019). It results in high $\delta^{15}N$ values of POM (6–8‰) and consequently higher $\delta^{15}N$ values of SOM. It is observed that the $\delta^{15}N$ value of SOM is more than 6‰ in sediments underlying the denitrification zones in the Arabian Sea (Gaye-Haake et al., 2005; Tripathi et al., 2017, 2020). In contrast, where denitrification is not prevalent, such as in the Bay of Bengal, the $\delta^{15}N$ value of SOM is 5–6‰ (Gaye-Haake et al., 2005). Denitrification also occurs in the pore waters of sediments, but the isotope effect is negligible ($\varepsilon \leq 0–3‰$) owing to the complete consumption of NO_3^- (Sigman et al., 2009). Naqvi et al. (1982) reported that the intensity of denitrification decreases gradually, corresponding to the dissolved oxygen's spatial distribution from the northern to the southern parts of the Arabian Sea, up to 12°N. The dissolved oxygen concentration decreases from south to north (Supplementary Fig. 1a). The N* also mimics the pattern shown by the dissolved oxygen, with low anomalies spreading beyond 12°N, implying significant denitrification (Supplementary Fig. 1d).

Another newly identified process of fixed nitrogen (i.e., biologically available nitrogen) removal is anammox, where NO_2^- oxidizes NH_4^+ to N_2 gas and NO_3^-. The isotopic effects arising out of anammox are not well understood, but a few available studies indicate an isotope effect of 23.5–30‰ (Brunner et al., 2013; Kobayashi et al., 2019). Nevertheless, such studies also note that the isotope effect derived for denitrification also includes the anammox effect, which probably increases the overall isotope effect, resulting in high $\delta^{15}N$ of PON (Brunner et al., 2013). Thus, the $\delta^{15}N$ value of the surface NO_3^- and the resulting organic matter preserved in the sediment in SEAS is predominantly governed by water column denitrification.

MATERIALS AND METHODOLOGY

Core details, chronology, and sedimentation rate

For the present study, sediment core SK274-4 G (13°59′N, 72°E; 2.60 m length) (Fig. 1), collected from the continental slope of SEAS during the 274th cruise of the ORV Sagar Kanya, is used. This core was retrieved using a gravity corer from a water depth of 1290 m within the present-day OMZ. The core was then subsampled at every 1-cm interval and freeze-dried for further analysis. The chronology of the core is based on nine radiocarbon dates obtained using two

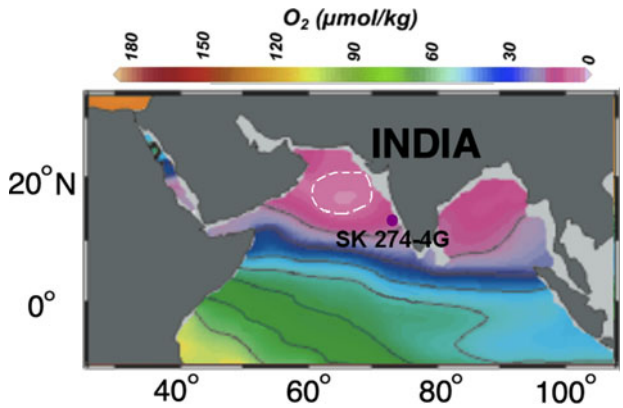

Figure 1. Location of core SK 274-4 G with contours showing dissolved oxygen concentration at 300 m depth. The white dashed line indicates the nitrite maximum (>0.5 µM/L; Naqvi and Noronha, 1991) coinciding with the lowest oxygen concentration. The pink color indicates the permanent oxygen minimum zone (O_2 <20 µM/kg). The dark pink circle indicates the location of core SK 274-4G. (For interpretation of the references to color in this figure legend, the reader is referred to the web version of this article.)

https://doi.org/10.1017/qua.2020.118 Published online by Cambridge University Press

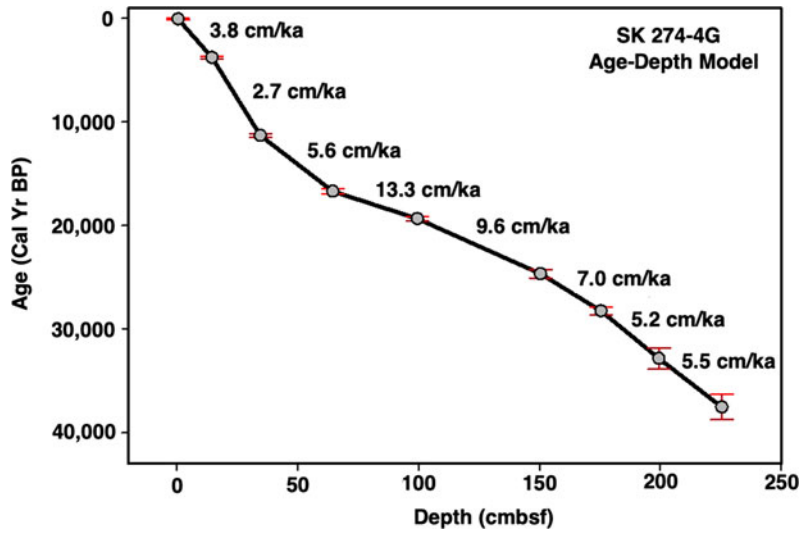

Figure 2. (color online) Age-depth model for core SK 274-4 G based on nine radiocarbon dates from selected species of planktic foraminifera. Sedimentation rates are shown in cm/ka.

species of planktic foraminifera (*Globigerinoides ruber* and *Globigerinoides sacculifer*; size range: 250–420 µm). The dates were obtained using the accelerator mass spectrometry (AMS) technique at the National Science Foundation AMS facility at the University of Arizona. The ^{14}C dates were calibrated using the marine dataset (Marine09) (Reimer et al., 2009) in Calib 6.0 (Stuiver and Reimer, 1993). The reservoir age correction of 355 years determined by Butzin et al. (2005) was used for the core. The reservoir age given by Butzin et al. (2005) is an estimate of ocean radiocarbon reservoir ages, based on a three-dimensional global ocean circulation model, and hence are more accurate (Cao et al., 2007). Core SK274-4 G spans the last ~43 ka, and the its top shows an age of ~800 yr. The age-depth model for the core is shown in Figure 2. The sedimentation rate for SK274-4 G averages 6.6 cm/ka and varies from 2.7 to 13.3 cm/ka for the past 43 ka. The maximum sedimentation rate of 13.3 and 9.6 cm/ka is observed at 16.7–19.3 and 19.3–24.6 ka intervals, respectively. The average sample resolution is ~150 yr.

Elemental and isotopic analyses of sedimentary organic carbon and total nitrogen

Each subsample was oven-dried at 40°C and then homogenized by finely grinding it in an agate mortar. For total organic carbon (TOC) concentration and $\delta^{13}C_{org}$ estimation, carbonate was removed from each subsample by treating it with 2N hydrochloric acid for 16 hours and then centrifuging it to remove carbonate. The samples were then completely rinsed by adding deionized water five times and again oven-dried at 40°C. Given the known problems of loss of nitrogen compounds from SOM on acidification of samples, resulting in a bias in nitrogen content and $\delta^{15}N$ values (Brodie et al., 2011), untreated samples were used for total nitrogen (TN) and $\delta^{15}N$ analyses. A portion of the ground samples was wrapped in a tin capsule and combusted using an elemental analyzer coupled to an Isoprime stable isotope ratio mass spectrometer at the Marine Stable Isotope Laboratory at the National Centre for Polar and Ocean Research (NCPOR), Goa, India. Samples were run along with blank and known standards. Standards were prepared by weighing 0.4–0.6 mg of IAEA cellulose (IAEA-CH-3) of certified isotopic composition ($\delta^{13}C = -24.74‰$ vs. the Vienna Pee Dee Belemnite [VPDB]) for carbon and 0.5–1.0 mg of IAEA ammonium sulphate (IAEA N1) of certified isotopic composition ($\delta^{15}N = 0.4‰$) for nitrogen. Carbon and nitrogen isotopic data are presented in δ notation with respect to the VPDB and atmospheric nitrogen, respectively. The analytical precisions based on repeat measurements of the reference standard for isotopic composition for the core are better than 0.02‰ for carbon and 0.08‰ for nitrogen. Analytical precisions based on repeat measurements of the reference standard (Sulfanilamide) for the TOC and TN measurements are ± 0.2% and ± 0.3%, respectively. Data quality was controlled by running the reference standard after every six samples.

Micropaleontological analysis

A total of 62 samples were selected at 5-cm intervals for the *Globigerina bulloides* abundance study. Each sample was weighed and wet-sieved over a 63-µm sieve. The residues were dried in an oven at 60°C, weighed, dry-sieved over a 125-µm screen, and then split into several aliquots to reduce the total number of foraminifera tests. In each sample, the faunal composition of planktic foraminifera was determined based on a minimum count of 300 individuals larger than 125 µm in diameter. The number of *G. bulloides* and the total number of planktic foraminifera for each sample was then counted. Finally, the relative abundance of *G. bulloides*

https://doi.org/10.1017/qua.2020.118 Published online by Cambridge University Press

was calculated as a percent of the total planktic foraminifera population.

RESULTS AND DISCUSSION

Surface water productivity during the last ~43 ka

An increased abundance of *G. bulloides* is indicative of upwelling of cold and nutrient-rich water to the surface, resulting in increased biological productivity. The upwelling is tightly coupled to productivity in the Arabian Sea, which is well established based on several sediment traps, plankton nets, remote sensing, and sediment core studies (Nair et al., 1989 and references therein). Therefore, changes in the abundance of *G. bulloides* can be an indicator of variability in productivity (Bé and Tolderlund, 1971; Kroon, 1988; Conan and Brummer, 2000; Singh et al., 2011).

In the present study, the *G. bulloides* abundance varies mostly between 5 and 20%. It was low during the glacial period and shows an increase during the deglaciation, with a decline during the Holocene (Fig. 3a). During the Last Glacial Maximum (LGM) and Henrich events (H1 to H4), it was low, suggesting decreased surface water productivity in SEAS. Most of the earlier studies from the eastern Arabian Sea report high glacial productivity, which has been attributed to a strong winter monsoon season, leading to enhanced convective mixing (Anil Kumar et al., 2005; Dahl and Oppo, 2006; Singh et al., 2006, 2011; Anand et al., 2008). A similar mechanism is unlikely to have occurred in SEAS because a significant increase in productivity in this region is observed only during the southwest monsoon season (Lévy et al., 2007). The weaker summer monsoon winds during the glacial interval must have resulted in a diminished summer season upwelling, thereby resulting in a decrease in productivity. A repeated abrupt decrease in *G. bulloides* during cold intervals was also reported from the central-eastern Arabian Sea and was attributed to a reduced winter monsoon strength, resulting in the strong stratification witnessed today during the inter-monsoon months (Singh et al., 2011). In SEAS, this decline in productivity during cold intervals and the LGM is also attributed to stronger stratification. But the cause of this at this core site was likely due to a weaker summer

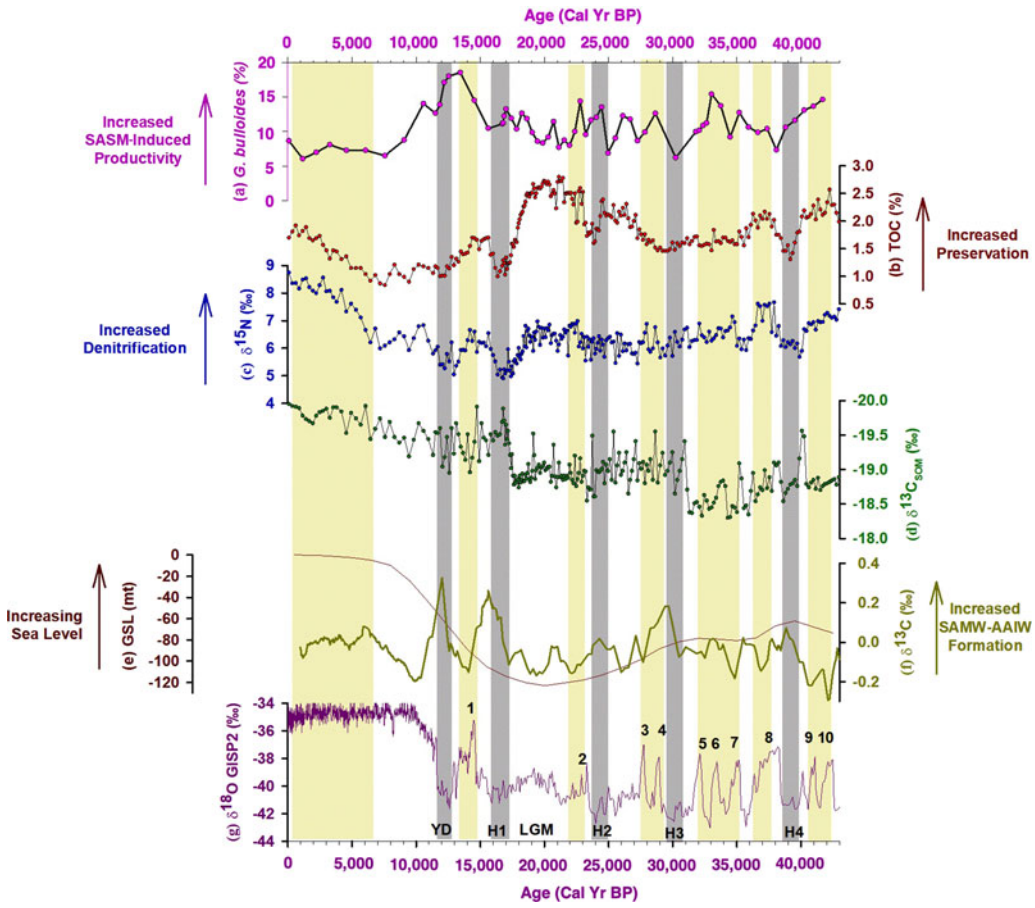

Figure 3. (color online) Downcore variation of geochemical proxies for core SK 274-4 G indicating productivity, denitrification, and provenance and its comparison with mean sea level, ventilation, and climate variability. Panels (a), (b), (c), and (d) show *Globigerina bulloides* abundance, total organic carbon concentration, $\delta^{15}N$, and $\delta^{13}C$ of the sedimentary organic matter, respectively, from the present study. Panel (e) shows the global mean sea-level variability (Siddall et al., 2003). Panel (f) shows the $\delta^{13}C$ of benthic foraminifera, indicating millennial-scale changes in the Sub-Antarctic Mode Water-Antarctic Intermediate Water formation rate (Jung et al., 2009). Panel (g) shows the Greenland Ice Sheet Project 2 (GISP2) $\delta^{18}O$ record (Blunier and Brook, 2001).

https://doi.org/10.1017/qua.2020.118 Published online by Cambridge University Press

monsoon season coupled with a continual supply of low-salinity Bay of Bengal waters (Sarkar et al., 1990) during the last glacial period, followed by the enhanced transport of these waters throughout the LGM (Saraswat et al., 2013; Naik et al., 2016). A major increase in *G. bulloides* abundance between 12 and 14.5 ka suggests an increase in surface water productivity similar to productivity changes estimated from other low- and mid-latitude upwelling areas (Agnihotri et al., 2003). Although we see a decline in *G. bulloides* abundance between 11.5 and 8.5 ka, the values were still higher than those seen after 7.5 ka. This higher abundance suggests comparatively higher productivity during the early Holocene in SEAS. It uniformly decreases during the Holocene, implying a gradual decrease in productivity, which is similar to that reported from core ODP 723A off the Oman margin (Anderson et al., 2010).

Provenance of organic matter at the study site

It is important to ascertain the sources of organic matter at the site before using it for studying past denitrification variability. The carbon isotopes of organic matter preserved in the sediment ($\delta^{13}C_{org}$) can help in identifying its provenance. Organic matter produced by marine algae has an average $\delta^{13}C_{org}$ value of ~ -21‰ (O'Leary, 1988; Farquhar et al., 1989). Whereas organic matter produced by land plants using the C3 pathway has an average $\delta^{13}C_{org}$ value of ~ -27‰, those using the C4 pathway is ~ -14‰ (O'Leary, 1988; Farquhar et al., 1989). In the present study, $\delta^{13}C_{org}$ varies from -20 to -18.30‰ (Fig. 3d). The $\delta^{13}C_{org}$ values show a decreasing trend from 40 ka to the present, but the values stay in the range of the marine organic matter values. This implies a predominantly marine origin for the organic matter at the site.

The TOC variability

The TOC concentration varies between 0.80 and 2.84% (Fig. 3b) and exhibits a similar variability to $\delta^{15}N$, with a higher concentration during warmer periods and a lower concentration during colder periods. However, in SEAS, decoupling between *G. bulloides* abundance and TOC, as shown in the present study, points toward factors other than productivity affecting TOC accumulation in sediments. A similar trend between $\delta^{15}N$ and TOC suggests that the accumulation of organic carbon in SEAS is mainly a response to better preservation under enhanced suboxic conditions rather than changes in primary productivity. In addition, a higher sedimentation rate can result in better preservation of organic matter, resulting in a higher TOC content (Calvert and Pedersen, 1993). Recently, Nagoji and Tiwari (2017) showed enhanced TOC values since the mid-Holocene, which was attributed to increased preservation caused by an increased sedimentation rate and enhanced reducing conditions in SEAS; this was also observed by Naik et al. (2014) and Agnihotri et al. (2003).

Centennial-scale denitrification variability in the eastern Arabian Sea

To determine the denitrification variability, we examined the $\delta^{15}N$ of the organic matter preserved in the sediment. Our analysis did not show any effect of diagenetic alteration and terrestrial organic matter on $\delta^{15}N$ values (see Supplementary Materials for more details). The $\delta^{15}N$ values vary between 8.74 and 4.91‰ (Fig. 3c). The present study finds higher $\delta^{15}N$ values during warmer periods (Marine Oxygen Isotope Stages [MIS] 1 and 3), indicating stronger denitrification and lower values, which in turn indicates weaker denitrification during the colder period (MIS 2). On shorter timescales, this high-resolution (centennial-scale) data show that the $\delta^{15}N$ values are high during the warm interstadials (Dansgaard-Oeschger events and since the mid-Holocene; shown by yellow bands in Fig. 3), indicating stronger denitrification. The $\delta^{15}N$ values are low during the cold stadials (Henrich events and Younger Dryas; shown by gray bands in Fig. 3), indicating weaker denitrification. We also observed moderately strong denitrification during the LGM.

The continuous wavelet transform (CWT) and the squared wavelet coherence (SWC), including phase analysis, was carried out to check if the visually perceived coherence between denitrification and climate is statistically significant (Fig. 4a and b), following Torrence and Campo (1998) and Grinsted et al. (2004). Figure 4a represents the CWT for $\delta^{15}N$ in SEAS. It shows high "power" in the periodicities between 1500 and 2000 years and between 3000 and 4000 years. These are very near to the well-known quasiperiodic variations of 1500 and 3000 years (Dansgaard-Oeschger events and Bond cycles) in various climate records. This suggests a strong coupling between denitrification and millennial-scale climate variability. The SWC also shows that denitrification intensity ($\delta^{15}N$ values) and climate variability (Greenland Ice Sheet Project 2 [GISP2] $\delta^{18}O$; Blunier and Brook, 2001) are statistically significantly coherent (5% significance level; Fig. 4b). The phase difference is represented by the vector; arrows pointing to the right indicate in-phase, which confirms the visual observations that whenever the $\delta^{15}N$ of organic matter is high (stronger denitrification in the Arabian Sea), the GISP2 $\delta^{18}O$ is also high (warmer climate).

One crucial limitation in assigning clear causes of denitrification changes in the OMZ is the lack of definite proxies for oxygen demand or supply. It has been noted that denitrification is most intense in the northeastern Arabian Sea (Naqvi, 1987). By itself, this would suggest corresponding geographical gradients in the sediment $\delta^{15}N$ signature. The water column data, in contrast, indicate a regional homogenization of the $\delta^{15}N$ signal that reaches the euphotic zone (e.g., Altabet et al., 2002). This regional homogeneity in the $\delta^{15}N$ signal in the Arabian Sea suggests two things. First, an effective horizontal mixing of thermocline water leads to homogenization of the $\delta^{15}N$ signals on the glacial-interglacial timescale. And second, local decoupling of productivity and denitrification exists and is probably due to effective ventilation of the thermocline. Pichevin et al (2007) compared the long-term, high-

https://doi.org/10.1017/qua.2020.118 Published online by Cambridge University Press

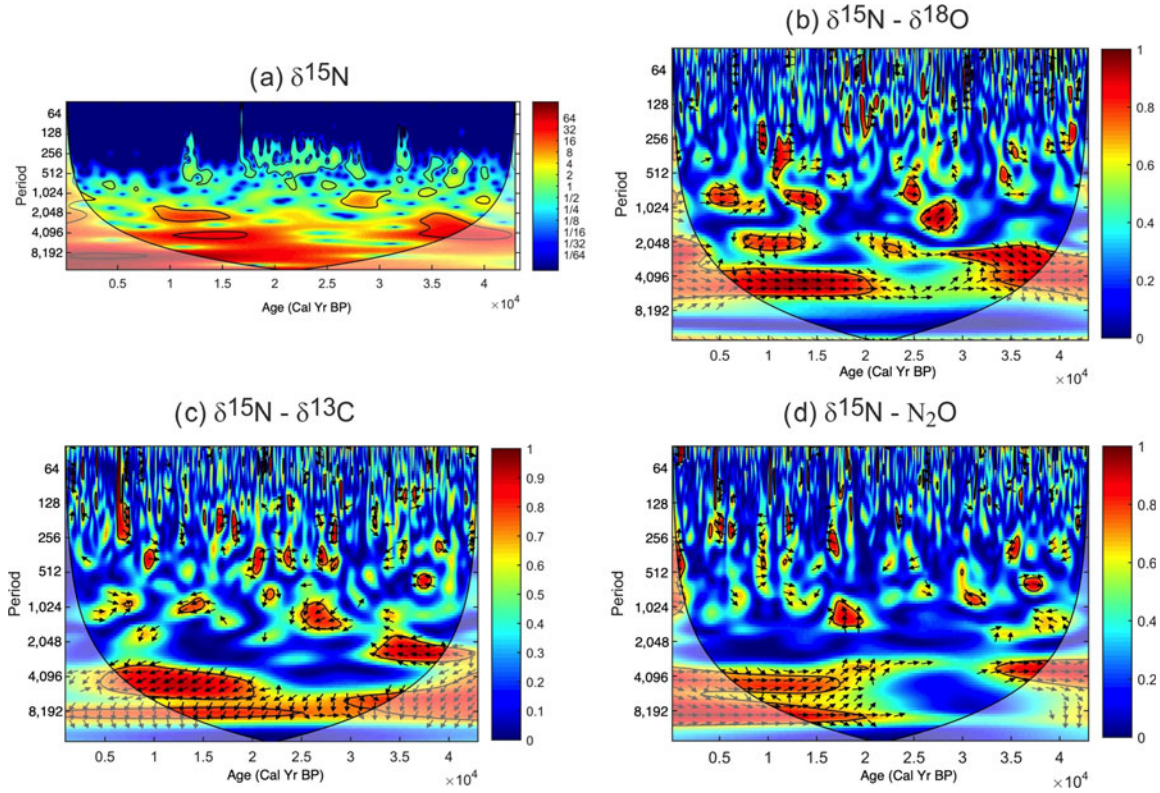

Figure 4. (color online) Spectral analyses, including the continuous wavelet transform (CWT) and the squared wavelet coherence (SWC). Panel (a) shows the CWT power spectrum for the denitrification variability ($\delta^{15}N$ of core SK 274-4G). Panel (b) shows the SWC between denitrification and climate ($\delta^{15}N$ and GISP2 $\delta^{18}O$). Panel (c) shows the SWC between denitrification and ventilation ($\delta^{15}N$ and $\delta^{13}C$). Panel (d) shows the SWC between denitrification and N_2O abundance ($\delta^{15}N$ and N_2O). The colors represents the "power," which is proportional to the amplitude of a wave of a given period. Phase arrows pointing to the right = in-phase, left-pointing arrows = antiphase, down-pointing arrows = $\delta^{15}N$ leading by 90°, and up-pointing arrows = $\delta^{15}N$ lagging by 90°. The 5% significance level against red noise is shown as a thick contour. The lighter shades depict the cone of influence. The x-axis spans the last 40,000 years as shown by $\times 10^4$.

resolution sedimentary $\delta^{15}N$ record on the glacial-interglacial timescale from the Arabian Sea and reported a spatial and temporal heterogeneity in denitrification, thus ruling out the first possibility. Therefore, the second possibility of local decoupling of productivity and denitrification is examined below.

Decoupling of surface ocean productivity and denitrification in SEAS during the LGM and the Holocene

The productivity variability is not always accompanied by similar denitrification variability in SEAS (Fig. 3a and c). This decoupling is more prominent during the LGM and since the early Holocene. The increase in surface water productivity and the associated oxygen demand for the degradation of organic matter produced is regarded as the main control of water column denitrification (Ganeshram et al., 2000; Ivanochko et al., 2005). Studies have proposed that ventilation of the thermocline by intermediate water masses also controls the denitrification intensity by modulating the oxygen supply (Sarma, 2002; Pichevin et al., 2007). Model studies have also shown that past changes in the ventilation rate at intermediate depth by the Antarctic Intermediate Water (AAIW) can modulate denitrification in the OMZ (Galbraith et al., 2004; Meissner et al., 2005; Schmittner et al., 2007), such as in the Arabian Sea. Given the decoupling between denitrification and productivity during the LGM and since the mid-Holocene in SEAS, we explore the impact of ventilation on the intensity of denitrification in this region below.

The cooling of high-latitude surface ocean waters and enhanced ventilation rates during the glacials could result in suppressing suboxic conditions and thus reduce water column denitrification (Meissner et al., 2005). In the western and northeastern Arabian Sea, studies have concluded that higher oxygen was related to an increased production of intermediate waters and its northward expansion (i.e., Sub-Antarctic Mode Water [SAMW]-AAIW) during North Atlantic Heinrich events (Pichevin et al., 2007). Therefore, to further investigate the influence of this southern-sourced, oxygen-rich intermediate-depth water mass in SEAS, we compared our $\delta^{15}N$ record with the carbon isotopes of the epibenthic foraminifera record from core NIOP 905, off the Somali coast (Fig. 3f) (Jung et al., 2009). The $\delta^{13}C$ value of epibenthic

https://doi.org/10.1017/qua.2020.118 Published online by Cambridge University Press

foraminifera serves as a proxy for ageing the water mass along its flow path, (i.e., the ventilation state of the ocean) (Pahnke and Zahn, 2005). The AAIW has a high $\delta^{13}C$ value of the dissolved inorganic carbon in the modern Indian and Pacific Oceans and was probably also high in the past (Charles and Fairbanks, 1992). The higher $\delta^{13}C$ values thus represent an increased SAMW-AAIW formation.

The comparison between low and high peaks in $\delta^{13}C$ values, suggesting decreased and increased SAMW-AAIW formation, and the $\delta^{15}N$ record of the present study reveals that during the last glacial-interglacial cycle, the high/low peaks in the $\delta^{15}N$ record are concurrent with episodes of decreased/increased SAMW-AAIW formation. Interestingly, the higher values observed in the $\delta^{15}N$ record during the LGM coincide with the major decline in the inflow of the SAMW-AAIW into the Arabian Sea, as evidenced by the low $\delta^{13}C$ value of epibenthic foraminifera. The lower $\delta^{15}N$ values were observed during Heinrich Event 1; during the Younger Dryas, they coincide with an enhanced inflow of the oxygen-rich water mass. However, beyond the early Holocene (after ~8 ka, in the Northgrippian), the observed relationship between the SAMW-AAIW flux and $\delta^{15}N$ weakens. This could be due to the presence of Indonesian intermediate, Red Sea, and Persian Gulf water masses, which were reduced during the last glacial period owing to an overall lower sea level (Kuhnt et al., 2004). During the last glacial period, when the sea level was 120 m lower than it is today (Fig. 3e), the Red Sea outflow (separated from the open ocean by shallow and narrow sills of 137 m) and the Persian Gulf outflow (separated from the open ocean by shallow and narrow sills of <100 m) was reduced by 85% (Rohling and Zachariasse, 1996). It reached 50% at 10 ka and increased progressively with sea-level rise thereafter until it reached its present state at ~6 ka (Fig. 3e) (Rohling and Zachariasse, 1996). So, during the last glacial-interglacial cycle, the intensity of denitrification at the core site was controlled by both the SASM-induced productivity and the southern-sourced oxygen-rich intermediate-depth water mass, with the latter dominating during the LGM. However, with the rise in sea level, the oxygen-poor Red Sea and Persian Gulf waters further prevented the southern-sourced water (SAMW-AAIW) from ventilating the Arabian Sea. It enabled a continuous buildup of oxygen deficiency and intensification of the OMZ and denitrification in the intermediate depth of SEAS. It also implies that the denitrification increase during the Holocene, which is often interpreted as strengthening the SASM, is in fact because of enhanced inflow of oxygen-poor water at intermediate depth. During the Holocene and the LGM, denitrification does not reflect the SASM-induced productivity.

The wavelet coherency analysis and the phase analysis were carried out to check if the visually perceived coherence between denitrification and the SAMW-AAIW formation is statistically significant (Fig. 4c), following Grinsted et al. (2004) and Torrence and Campo (1998). We find that the denitrification intensity is statistically significantly coherent (5% significance level), with the SAMW-AAIW formation over a periodicity band of ~1000, 2000, 4000, and 8000 years during the different parts of the time series as shown in Figure 4c. The vector represents the phase difference; the arrows pointing to the left indicate antiphase, which confirms the visual observations; i.e., higher denitrification (high $\delta^{15}N$) during reduced SAMW-AAIW inflow (low benthic foraminifera $\delta^{13}C$).

Teleconnection among denitrification, high-latitude climate, and global monsoon: a probable mechanism

Denitrification generates nitrous oxide (N_2O), an important greenhouse gas (Naqvi et. al., 2006). Today, the oceans are one of the most important natural sources of N_2O, supplying up to an estimated 5.4 Tg N/yr of which upwelling is a significant contributor (United States Environmental Protection Agency, 2010). For example, SASM-induced upwelling in the northwestern Arabian Sea, covering only 0.43% of the global oceans, contributes up to 18% of the total oceanic flux of N_2O (Law and Owens, 1990). We find that higher and lower denitrification intensity observed in the present study matches with higher and lower N_2O concentrations, respectively, in the central Greenland ice cores (GISP2; Sowers et al., 2003) within the constraints of the different resolutions (Fig. 5a and b). The high-resolution N_2O data from these ice cores (from the Greenland Ice Core Project and the North Greenland Ice Core Project; Flückiger et al., 2004) also show a close correspondence with the denitrification variability during MIS 3 within the chronological uncertainties. This appears to break down during the Holocene. Possibly, denitrification is so intense (evident from the very high $\delta^{15}N$ values) that a relatively larger proportion of N_2O is further reduced to N_2 gas.

The visual similarity between N_2O (Sowers et al., 2003) and the denitrification variability (present study) is further statistically confirmed by wavelet coherency analysis and phase analysis (Fig. 4d). We find that the denitrification intensity and N_2O record are statistically significantly coherent (5% significance level) over a periodicity band of ~4000 and 8000 years. The vector represents the phase difference; the arrows pointing to the right indicate in-phase, which confirms the visual observations. This coupling between high and low denitrification and high and low N_2O abundance is observed during warm and cold periods, respectively, and is identified through the $\delta^{18}O$ record of the GISP2 ice core (Fig. 5j). It implies that a part of global warmth due to higher greenhouse gases abundance can be ascribed to the tropical denitrification variability.

We further compared our $\delta^{15}N$ record with a set of key paleomonsoon records located at the northern rim of the boreal summer Intertropical Convergence Zone (ITCZ) monsoonal rain belt for the past 40 ka (Fig. 5). All of them show increased intensity during warm interstadials and decreased intensity during cold stadials. Similar variability during warm and cold periods in a well-dated, high-resolution record from a stalagmite from Dongge cave (Cheng et al.,

https://doi.org/10.1017/qua.2020.118 Published online by Cambridge University Press

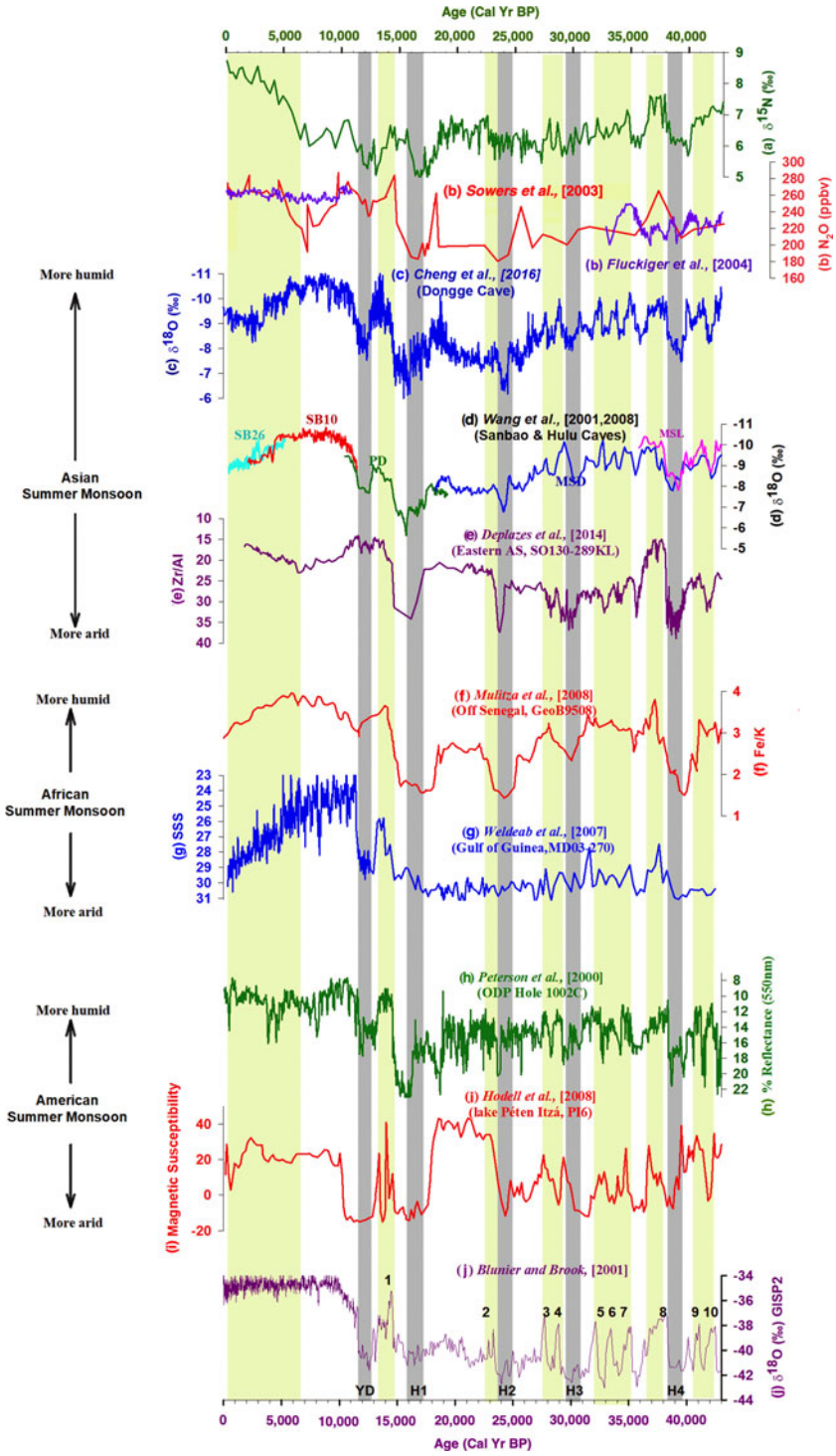

Figure 5. Comparison of denitrification in the Arabian Sea with atmospheric N_2O abundance, as reflected in the central Greenland ice cores record and the global summer monsoon convection and precipitation. The yellow and gray vertical bands show warmer and colder periods, respectively. Panel (a) shows denitrification in the southeastern Arabian Sea (present study). Panel (b) shows N_2O variability of the central Greenland ice cores (Sowers et al., 2003; Flückiger et al., 2004). Panel (c) shows the stalagmite $\delta^{18}O$ records from Dongge cave (Cheng et al., 2016). Panel (d) shows the stalagmite $\delta^{18}O$ records from Hulu cave (Wang et al., 2001) and Sanbao cave (SB26 = sky blue, SB10 = red) (Wang et al., 2008). Panel (e) shows the elemental ratio of zirconium to aluminum (Zr/Al) from the northern Arabian Sea, reflecting grain size, source aridity, and wind strength (Deplazes et al., 2014), and indicating the intensity of the Asian summer monsoon. Panel (f) shows the elemental ratio of iron to potassium (Fe/K) in core GeoB9508 off the coast of Senegal, tracing Sahel aridity (Mulitza et al., 2008). Panel (g) shows the sea surface salinity record from the Gulf of Guinea, suggesting relative changes in the outflow of the Niger and Sanaga Rivers (Weldeab et al., 2007) and reflecting the intensity of the African summer monsoon. Panel (h) shows downcore color reflectance measurements from the Cariaco Basin (Peterson et al., 2000). Panel (i) shows the magnetic susceptibility in Lake Péten Itzá, Guatemala (Hodell et al., 2008), reflecting the intensity of the American summer monsoon. Panel (j) shows the GISP2 $\delta^{18}O$ records (Blunier and Brook, 2001). (For interpretation of the references to color in this figure legend, the reader is referred to the web version of this article.)

https://doi.org/10.1017/qua.2020.118 Published online by Cambridge University Press

2016) and another from Hulu and Sanbao caves (Wang et al., 2001, 2008) (Fig. 5c and d), along with one from the northern Arabian Sea (Fig. 5e) (Deplazes et al. 2014), suggests that millennial-scale changes in the intensity of the Asian monsoon occurred synchronously with changes in the North Atlantic. Based on the relative contributions of atmospheric dust and fluvial suspension in marine sediments using the elemental ratio of iron to potassium (Fe/K) (Fig. 5f), Mulitza et al. (2008) suggested abrupt onsets of arid conditions in the West African Sahel during the time of Henrich events. Further, the precipitation record from the marine sediment core in the Gulf of Guinea (MD03-270), an indicator of relative changes in the outflow of the Niger and Sanaga Rivers, shows a decline during cold stadials and from the mid-Holocene to the present (Weldeab et al., 2007) (Fig. 5g). In the Cariaco Basin, at the northern extent of the South American ITCZ seasonal migration, Peterson et al., (2000) noted downcore color reflectance measurements (ODP site 1002C) (Fig. 5h) that register millennial-scale variation in the ITCZ position. They also observed deposition of dark, generally laminated, sediments during warm interstadial intervals, whereas deposition of light-colored bioturbated sediments was restricted to colder stadial intervals of the last glacial. Hodell et al. (2008) examined magnetic susceptibility, reflecting wet-dry cycles (Fig. 5i). The most arid conditions were observed during Heinrich events, which accords with the results from the Cariaco Basin (Peterson et al., 2000). Thus, the above comparisons reveal that the major periods of increased global monsoon intensity covaried and were accompanied by enhanced denitrification/N_2O emission. Additionally, tropical precipitation leads to larger wetlands, the most important source of methane. Present-day estimates suggest that natural wetlands contribute 170 Tg CH_4/yr (United States Environmental Protection Agency, 2010). Thus, enhanced tropical monsoon convection appears to increase the production of greenhouse gases. Further, studies from the western Arabian Sea have shown that the denitrification variability may affect the atmospheric CO_2 via modulation of the biological pump through changes in the marine nitrogen inventory (Altabet et al., 2002; Ganeshram et al., 2002). Hence, the synchronicity between the high-latitude climate, denitrification, and the global monsoon system (South American, African, and Asian monsoons) at the millennial timescale indicates that variations in tropical monsoonal convection possibly affect the atmospheric moisture content and emission of greenhouse gases, which in turn influence the high-latitude climate.

CONCLUSIONS

This study presents the centennial-scale denitrification variability from SEAS since the last glacial period. It finds a close correspondence between millennial-scale climate change and denitrification. Stronger denitrification is observed during warm periods and Dansgaard-Oeschger events. Weaker denitrification is found during cold periods (except the LGM) like Heinrich events and the Younger Dryas. It demonstrates that both the ventilation of the SAMW-AAIW and the SASM-induced productivity played a crucial role in modulating denitrification intensity in SEAS. During the Holocene and the LGM, denitrification increased (higher $\delta^{15}N$) despite reduced monsoon-induced productivity in SEAS. During the LGM, this increased intensity is related to reduced thermocline ventilation as a result of weakened thermohaline circulation. Conversely, during the Holocene, the decoupling between denitrification and productivity is caused by the sluggish inflow of oxygen-depleted Red Sea and Persian Gulf waters into the intermediate depth of SEAS owing to rising sea level. Thus, increasing denitrification during the Holocene does not reflect higher productivity and hence does not suggest strengthening SASM. Finally, this study shows that tropical convection and denitrification influenced the high-latitude climate on the millennial timescale through significant greenhouse gas production.

ACKNOWLEDGMENTS

We thank the director of the NCPOR for support and encouragement. Tiwari also thanks the Ministry of Earth Sciences, the Government of India, and the Research Council of Norway for support through the Ind-Nor program (MoES/Ind-Nor/PS-8/2015 and grant no. 248793). We thank M. Tariq of NCPOR for help in spectral analysis and C. Torrence, G.P. Compo, A. Grinsted, J.C. Moore, and S. Jevrejeva for MATLAB codes. We thank the two anonymous reviewers, and editors D. Booth and L. Bradtmiller, for constructive comments.The data for this paper can be accessed through the supporting information or by direct request to the corresponding author. This is NCPOR contribution no. J-79/2020-21.

SUPPLEMENTARY MATERIAL

The supplementary material for this article can be found at https://doi.org/10.1017/qua.2020.118

REFERENCES CITED

Agnihotri, R., Bhattacharya, S.K., Sarin, M.M., Somayajulu, B.L.K., 2003. Changes in surface productivity and subsurface denitrification during the Holocene: a multiproxy study from the eastern Arabian Sea. *The Holocene* 13, 701–713.

Altabet, M.A., Francois, R., Murray, D.W., Prell, W.L., 1995. Climate related variations in denitrification in the Arabian Sea from sediment 15N/14N ratios. *Nature* 373, 506–509.

Altabet, M.A., Higginson, M.J., Murray, D.W., 2002. The effect of millennial-scale changes in Arabian Sea denitrification on atmospheric CO_2. *Nature* 415, 159–162.

Altabet, M.A., Murray, D.W., Prell, W.L., 1999. Climatically linked oscillations in Arabian Sea denitrification over the past 1 m.y.: implications for the marine N cycle. *Paleoceanography* 14, 732–743.

Anand, P., Kroon, D., Singh, A.D., Ganeshram, R.S., Ganssen, G., Elderfield, H., 2008. Coupled sea surface temperature-seawater $\delta^{18}O$ reconstructions in the Arabian Sea at the millennial scale for the last 35 ka. *Paleoceanography* 23, 4207.

Anderson, D.M., Baulcomb, C.K., Duvivier, A.K., Gupta A.K., 2010. Indian summer monsoon during the last two millennia. *Journal of Quaternary Science* 25, 911–917.

Anil Kumar, A., Rao, V.P., Patil, S.K., Kessarkar, P.M., Thamban, M., 2005. Rock magnetic records of the sediments of the eastern Arabian Sea: evidence for late Quaternary climatic change. *Marine Geology* 220, 59–82.

Banse, 1987. Seasonality in phytoplankton chlorophyll in the central and northern Arabian Sea. *Deep Sea Research I* 34, 713–723.

Banse, K., Naqvi, S.W. A., Narvekar, P.V., Postel, J.R., Jayakumar, D.A., 2014. Oxygen minimum zone of the open Arabian Sea: variability of oxygen and nitrite from daily to decadal timescales. *Biogeosciences* 11, 2237–2261.

Bé, A.W.H., Tolderlund, D.S., 1971. Distribution and ecology of living planktonic foraminifera in surface waters of the Atlantic and Indian Oceans. In: Funnell, B.M., Riedel, W.R. (Eds.), *The Micropaleontology of Oceans*. Cambridge University Press, Cambridge, U.K., pp. 105–149.

Bhattathiri, P.M.A., Pant, A., Sawant, S., Gauns, M., Matondakar, S.G.P., Mohanraju, R., 1996. Phytoplankton production and chlorophyll distribution in the eastern and central Arabian Sea in 1994–1995. *Current Science* 71, 857–862.

Blunier, T., Brook, E.J., 2001. Timing of millennial-scale climate change in Antarctica and Greenland during the last glacial period. *Science* 291, 109–112.

Brandes J.A., Devol A.H., 2002. A global marine-fixed nitrogen isotopic budget: implications for Holocene nitrogen cycling. *Global Biogeochemical Cycles* 16, 1–14.

Brandes, J.A., Devol, A.H., Yoshinari, T., Jayakumar, D.A., Naqvi, S.W.A., 1998. Isotopic composition of nitrate in the central Arabian Sea and eastern tropical North Pacific: a tracer for mixing and nitrogen cycles. *Limnology and Oceanography* 43, 1680–1689.

Brodie, C.R., Casford, J.S.L., Lloyd, J.M., Leng, M.J., Heaton, T.H.E., Kendrick, C.P., Zong, Y.Q., 2011. Evidence for bias in C/N, $\delta^{13}C$ and $\delta^{15}N$ values of bulk organic matter, and on environmental interpretation, from a lake sedimentary sequence by pre-analysis acid treatment methods. *Quaternary Science Review* 30, 3076–3087.

Broecker, W.S., Peteet, D.M., Rind, D., 1985. Does the ocean-atmosphere system have more than one mode of operation? *Nature* 315, 21–26.

Brunner, B., Contreras, S., Lehmann, M.F., Matantseva, O., Rollog, M., Kalvelage, T., Klockgether, G., *et al*.., 2013. Nitrogen isotope effects induced by anammox bacteria. *Proceedings of the National Academy of Sciences* 110, 18994–18999.

Butzin, M., Prange, M., Lohmann, G., 2005. Radiocarbon simulations for the glacial ocean: the effects of wind stress, southern ocean sea ice and Heinrich events. *Earth Planetary Science Letters* 235, 45–61.

Calvert, S.A.E., Pedersen, T.F., 1993. Geochemistry of recent oxic and anoxic sediments: implications for the geological record. *Marine Geology* 113, 67–88.

Cao, L., Fairbanks, R.G., Mortlock, R.A., Risk, M.J., 2007. Radiocarbon reservoir age of high latitude North Atlantic surface water during the last deglacial. *Quaternary Science Review* 26, 732–742.

Capone, D.G., Subramaniam, A., Montoya, J.P., Voss, M., Humborg, C., Johansen, A.M., Siefert, R.L., Carpenter, E.J., 1998. An extensive bloom of the N_2-fixing cyanobacterium Trichodesmium erythraeum in the central Arabian Sea. *Marine Ecology Progress* 172, 281–292.

Charles, C.D., Fairbanks, R.G., 1992. Evidence from southern ocean sediments for the effect of North Atlantic deep water flux on climate. *Nature* 355, 416–419.

Cheng, H.R., Edwards, L., Sinha, A., Spötl, C., Yi, L., Chen, S., Kelly, M., *et al*., 2016. The Asian monsoon over the past 640,000 years and ice age terminations. *Nature* 534, 640–646.

Codispoti, L.A., Brandes, J.A., Christensen, J.P., Devol, A.H., Naqvi, S.W.A., Paerl, H.W., Yoshinari, T., 2001. The oceanic fixed nitrogen and nitrous oxide budgets: moving targets as we enter the anthropocene? *Scientia Marina* 65, 85–105.

Conan, S.M.H., Brummer, G.J., 2000. Fluxes of planktonic foraminifera in response to monsoonal upwelling on the Somalia Basin margin. *Deep Sea Research Part II* 47, 2207–2227.

Dahl, K.A., Oppo, D.W., 2006. Sea surface temperature pattern reconstructions in the Arabian Sea. *Paleoceanography* 21, 1014.

Deplazes, G., Lückge, A., Stuut, J.B.W., Pätzold, J., Kuhlmann, H., Husson, D., Fant, M., Haug, G.H., 2014. Weakening and strengthening of the Indian monsoon during Heinrich events and Dansgaard-Oeschger oscillations. *Paleoceanography* 29, 99–114.

Farquhar, G.D., Ehleringer, J.R., Hubick, K.T., 1989. Carbon isotope discrimination and photosynthesis. *Annual Review of Plant Physiology and Plant Molecular Biology* 40, 503–537.

Flückiger, J., Blunier, T., Stauffer, B., Chappellaz, J., Spahni, R., Kawamura, K., Schwander, J., Stocker, T.F., Dahl-Jensen, D., 2004. N_2O and CH_4 variations during the last glacial epoch: insight into global processes. *Global Biogeochemical Cycles* 18, 1020.

Fontugne, M.R., Duplessy, J.C., 1986. Variations of the monsoon regime during the upper Quaternary: evidence from carbon isotopic record of organic matter in North Indian Ocean sediment cores. *Palaeogeography, Palaeoclimatology, Palaeoecology* 56, 69–88.

Galbraith, E.D., Kienast, M., Pedersen, T.F., Calvert, S.E., 2004. Glacial-interglacial modulation of the marine nitrogen cycle by high-latitude O_2 supply to the global thermocline. *Paleoceanography* 19, 4007.

Ganeshram, R.S., Pedersen, T.F., Calvert, S.E., McNeil, G.W., 2000. Glacial-interglacial variability in denitrification in the world's oceans: causes and consequences. *Paleoceanography* 15, 361–376.

Ganeshram, R.S., Pedersen, T.F., Calvert, S.E., Murray, J.W., 1995. Large changes in oceanic nutrient inventories from glacial to interglacial periods. *Nature* 376, 755–758.

Ganeshram, R.S., Pederson, T.F., Calvert, S.E., Francois, R., 2002. Reducing nitrogen fixation in the glacial oceans inferred from changes in marine nitrogen and phosphate. *Nature* 415, 156–159.

Gaye-Haake, B., Lahajnar, N., Emeis, K.-C., Unger, D., Rixen, T., Suthhof, A., Ramaswamy, V., *et al*., 2005. Stable nitrogen isotopic ratios of sinking particles and sediments from the northern Indian Ocean. *Marine Chemistry* 96, 243–255.

Goswami, B.N., Venugopal, V., Sengupta, D., Madhosoodanan, M.S., Zavier, P.K., 2006. Increasing trend of extreme rain events over India in a warming environment. *Science* 314, 1442–1445.

Grinsted, A., Moore, J.C., Jevrejeva, S., 2004. Application of the cross wavelet transform and wavelet coherence to geophysical time series. *Nonlinear Processes in Geophysics* 11, 561–566.

Gruber, N., Sarmiento, J.L., 2002. Large-scale biogeochemical-physical interactions in elemental cycles. In: Robinson, A.R., McCarthy, J.J., Rothschild, B.J. (Eds.), *The Sea.* Vol. 12, *Biological-Physical Interactions in the Sea*. John Wiley and Sons Inc., New York, pp. 337–399.

Hodell, D.A., Anselmetti, F.S., Ariztegui, D., Brenner, M., Curtis, J.H., Gilli, A., Grzesik, D.A., *et al*., 2008. An 85-ka record of climate change in lowland Central America. *Quaternary Science Reviews* 27, 1152–1165.

https://doi.org/10.1017/qua.2020.118 Published online by Cambridge University Press

Howell, E.A., Dioney, S.C., Fine, R.A., Olson, D.B., 1997. Geochemical estimates of denitrification in the Arabian Sea and the Bay of Bengal during WOCE. *Geophysical Research Letters* 24, 2549–2552.

Ivanochko, T.S., Ganeshram, R.S., Brummer, G.J.A., Ganssen, G., Jung, S.J.A., Moreton, S.G., Kroon, D., 2005. Variations in tropical convection as an amplifier of global climate change at the millennial scale. *Earth and Planetary Science Letters* 235, 302–314.

Jung, S., Kroon, D., Ganssen, G., Peeters, F., 2009. Enhanced Arabian Sea intermediate water flow during glacial North Atlantic cold phases. *Earth and Planetary Science Letters* 280, 220–228.

Kessarkar, P.M., Rao, V.P., Naqvi, S.W.A., Karapurkar, S.G., 2013. Variation in the Indian summer monsoon intensity during the Bolling-Allerod and Holocene. *Paleoceanography* 28, 413–425.

Kobayashi, K., Makabe, A., Yano, M., Oshiki, M., Kindaichi, T., Casciotti, K.L., Okabe, S., 2019. Dual nitrogen and oxygen isotope fractionation during anaerobic ammonium oxidation by anammox bacteria. *The ISME Journal* 13, 2426–2436.

Kroon, D., 1988. The planktic $\delta^{13}C$ record, upwelling and climate. In: Brummer G.J.A., Kroon, D. (Eds.), *Planktonic Foraminifers as Tracers of Ocean-Climate History: Ontogeny, Relationships and Preservation of Modern Species and Stable Isotopes, Phenotypes and Assemblage Distribution in Different Water Masses*. Free University Press, Amsterdam, pp. 335–346.

Kudrass, H.R., Hofmann, A., Doose, H., Emeis, K., Erlenkeuser, H., 2001. Modulation and amplification of climatic changes in the Northern Hemisphere by the Indian summer monsoon during the past 80 k.y. *Geology* 29, 63–66.

Kuhnt, W., Holbourn, A.E., Hall, R., Zuleva, M., Kase, R., 2004. Cenozoic history of the Indonesian throughflow. In: Clift, P., Kuhnt, W., Wang, P., Hayes, D. (Eds.), *Continent-Ocean Interactions within East Asian Marginal Seas*. Geophysical Monograph Series 149. American Geophysical Union, Washington, D.C., pp. 287–308.

Law, C.S., Owens, N.J.P., 1990. Significant flux of atmospheric nitrous oxide from the northwest Indian Ocean. *Nature* 346, 826–828.

Lévy, M., Shankar, D., Andre, J.M., Shenoi, S.S.C., Durand, F., DeBoyer Montegut, C., 2007. Basin-wide seasonal evolution of the Indian Ocean's phytoplankton blooms. *Journal of Geophysical Research* 112, C12014.

Madhupratap, M., Prasanna Kumar, M.S., Bhattathiri, P.M.A., Dileep Kumar, M., Raghukumar, S., Nair, K.K.C., Ramaiah, N., 1996. Mechanism of the biological response to winter cooling in the northeastern Arabian Sea. *Nature* 384, 549–552.

Meissner, K.J., Galbraith, E.D., Volker, C., 2005. Denitrification under glacial and interglacial conditions: a physical approach. *Paleoceanography* 20, 3001.

Mulitza, S., Prange, M., Stuut, J.B., Zabel, M., von Dobeneck, T., Itambi, A.C., Nizou, J., Schulz, M., Wefer, G., 2008. Sahel mega droughts triggered by glacial slowdowns of Atlantic meridional overturning. *Paleoceanography* 23, 4206.

Nagoji, S.S., Tiwari, M., 2017. Organic carbon preservation in southeastern Arabian Sea sediments since mid-Holocene: implications to South Asian summer monsoon variability. *Geochemistry, Geophysics, Geosystems* 18, GC006804.

Naik, D.K., Saraswat, R., Lea, D.W., Kurtarkar, S.R., Mackensen, A., 2016. Last glacial-interglacial productivity and associated changes in the eastern Arabian Sea. *Palaeogeography, Palaeoclimatology, Palaeoecology* 483, 147–156.

Naik, S.S., Godad, S.P., Naidu, P.D., Tiwari, M., Paropkari, A.L., 2014. Early to late Holocene contrast in productivity, OMZ intensity and calcite dissolution in the eastern Arabian Sea. *The Holocene* 24, 749–755.

Nair, R.R., Ittekkot, V., Manganini, S.J., Ramaswamy, V., Haake, B., Degens, E.T., Desai, B. N., Honjo, S., 1989. Increased particle-flux to the deep ocean related to monsoons. *Nature* 338, 749–751.

Naqvi, S., Naik, H., Pratihary, A., D'Souza, W., Narvekar, P., Jayakumar, D., Devol, A., Yoshinari, T., Saino, T., 2006. Coastal versus open-ocean denitrification in the Arabian Sea. *Biogeoscience* 3, 621–633.

Naqvi S.W.A., 1987. Some aspects of the oxygen-deficient conditions and denitrification in the Arabian Sea. *Journal of Marine Research* 45, 1049–1072.

Naqvi, S.W.A., 1994. Denitrification processes in the Arabian Sea. *Proceedings of the Indian Academy of Sciences, Earth and Planetary Sciences* 103, 279–300.

Naqvi, S.W.A., Jayakumar, D.A., Narvekar, P.V., Naik, H., Sarma, V.S., D'Souza, W., Joseph, T., George, M.D., 2000. Increased marine production of N_2O due to intensifying anoxia on the Indian continental shelf. *Nature* 408, 346–349.

Naqvi S.W.A., Noronha, R.J., 1991. Nitrous oxide in the Arabian Sea. *Deep Sea Research* 38, 871–889.

Naqvi, S.W.A., Noronha, R.J., Reddy, C., 1982. Denitrification in the Arabian Sea. *Deep-Sea Research Part A. Oceanographic Research Papers* 29, 459–469.

O'Leary, M. H., 1988. Carbon isotopes in photosynthesis. *Bioscience* 38, 328–336.

Pahnke, K., Zahn, R., 2005. Southern Hemisphere water mass conversion linked with North Atlantic climate variability. *Science* 307, 1741–1746.

Paulmier, A., Ruiz-Pino, D., 2009. Oxygen minima zones (OMZs) in the modern ocean. *Progress in Oceanography* 80, 113–128.

Peterson, L.C., Haug, G.H., Hughen, K.A., Röhl, U., 2000. Rapid changes in the hydrologic cycle of the tropical Atlantic during the last glacial. *Science* 290, 1947–1951.

Pichevin, L., Bard, E., Martinez, P., Billy, I., 2007. Evidence of ventilation changes in the Arabian Sea during the Late Quaternary: implications for denitrification and nitrous oxide emission. *Global Biogeochemical Cycles* 21, GB4008.

Rafter, P.A., Bagnell, A., Marconi, D., DeVries, T., 2019. Global trends in marine nitrate N isotopes from observations and a neural network-based climatology. *Biogeosciences* 16, 2617–2633.

Reimer, P.J., Baillie, M.G.L., Bard, E., Bayliss, A., Beck, J.W., Blackwell, P.G., Bronk Ramsey, C., *et al*., 2009. Intcal09 and Marine09 radiocarbon age calibration curves, 0–50,000 years cal BP. *Radiocarbon* 51, 1111–1150.

Rohling, E.J., Zachariasse, W.J., 1996. Red Sea out flow during the last glacial maximum. *Quaternary International* 31, 77–83.

Saraswat, R., Lea, D.W., Nigam, R., Mackensen, A., Naik, D.K., 2013. Deglaciation in the tropical Indian Ocean driven by interplay between the regional monsoon and global teleconnections. *Earth Planetary Science Letters* 375, 166–175.

Sarkar, A., Ramesh, R., Bhattacharya, S.K., Rajagopalan, G., 1990. Oxygen isotope evidence for a stronger winter monsoon current during the last glaciation. *Nature* 343, 549–551.

Sarma, V.V.S.S., 2002. An evaluation of physical and biogeochemical processes regulating perennial suboxic conditions in the water column of the Arabian Sea. *Global Biogeochemical Cycles* 16, 1082.

Schäfer, P., Ittekkot, V., 1993. Seasonal variability of $\delta^{15}N$ in settling particles in the Arabian Sea and its palaeogeochemical significance. *Naturwissenschaften* 80, 511–513.

https://doi.org/10.1017/qua.2020.118 Published online by Cambridge University Press

Schmittner, A., Galbraith, E.D., Hostetler, S.W., Pedersen, T.F., Zhang, R., 2007. Large fluctuations of dissolved oxygen in the India and Pacific Oceans during Dansgaard-Oeschger oscillations caused by variations of North Atlantic deep water subduction. *Paleoceanography* 22, 3207.

Schulz, H., von Rad, U., Erlenkeuser, H., 1998. Correlation between Arabian Sea and Greenland climate oscillations of the past 110,000 years. *Nature* 393, 54–57.

Shenoi, S.S.C., Shankar, D., Shetye, S.R., 1999. The sea surface temperature high in the Lakshadweep Sea before the onset of the southwest monsoon. *Journal of Geophysical Research* 104, 703–712.

Siddall, M., Rohling, E., Almogi-Labin, A., Hemleben, Ch., Meischner, D., Schmelzer, I., Smeed, D.A., 2003. Sea-level fluctuations during the last glacial cycle. *Nature* 423, 853–858.

Sigman, D.M., Altabet, M. A., Michener, R.H., McCorkle, D.C., Fry, B., Holmes, R.M. 1997. Natural abundance-level measurement of the nitrogen isotopic composition of oceanic nitrate: an adaptation of the ammonia diffusion method. *Marine Chemistry* 57, 227–242.

Sigman, D.M., Karsh, K.L., Casciotti, K. L. 2009. Nitrogen isotopes in the ocean. In: Steele, J.H., Turekian, K.K., Thorpe, S.A. (Eds.), *Encyclopedia of Ocean Sciences*. Academic Press, London, 40–54.

Singh, A.D., Jung, S.J.A., Darling, K., Ganeshram, R., Ivanochko, T., Kroon, D., 2011. Productivity collapses in the Arabian Sea during glacial cold phases. *Paleoceanography* 26, PA3210.

Singh, A.D., Kroon, D., Ganeshram, R., 2006. Millennial scale variations in productivity and OMZ intensity in the eastern Arabian Sea. *Journal of Geological Society of India* 68, 369–377.

Sowers, T., Alley, R.B., Jubenville, J., 2003. Ice core records of atmospheric N_2O covering the last 106,000 years. *Science* 301, 945–948.

Stuiver, M., Reimer, P.J., 1993. Extended ^{14}C database and revised CALIB radiocarbon calibration program. *Radiocarbon* 35, 215–230.

Tiwari, M., Ramesh, R., Bhushan, R., Sheshshayee, M.S., Somayajulu, B.L.K., Jull, A.J.T., Burr, G.S., 2010. Did the Indo-Asian summer monsoon decrease during the Holocene following insolation? *Journal of Quaternary Science,* 25, 1179–1188.

Tiwari, M., Ramesh, R., Somayajulu, B.L.K., Jull, A.J.T., Burr, G.S., 2006. Paleomonsoon precipitation deduced from a sediment core from the equatorial Indian Ocean. *Geo-Marine Letters* 26, 23–30.

Torrence, C., Compo, G.P., 1998. A practical guide to wavelet analysis. *Bulletin of American Meteorological Society* 79, 61–78.

Tripathi, S., Behera, P., Tiwari, M., 2020. Evolution and dynamics of the denitrification in the Arabian Sea on millennial to million-year timescale. *Current Science* 119, 282–290.

Tripathi, S., Tiwari, M., Lee, J., Khim, B.K., IODP Expedition 355 Scientists, 2017. First evidence of denitrification vis-à-vis monsoon in the Arabian Sea since Late Miocene. *Scientific Reports* 7, 43056.

United States Environmental Protection Agency, 2010. *Methane and Nitrous Oxide Emissions from Natural Sources*. EPA 430-R-10-001, Office of Atmospheric Programs, Washington, D.C.,

Wang, H., Liu, H., Cui, H., Abrahamsen, N., 2001. Terminal Pleistocene/Holocene palaeoenvironmental changes revealed by mineral-magnetism measurements of lake sediments for Dali Nor area, southeastern inner Mongolia plateau, China. *Palaeogeography, Palaeoclimatology, Palaeoecology* 170, 115–132.

Wang, Y., Cheng, H., Edwards, R.L., Kong, X., Shao, X., Chen, S., Wu, J., Jiang, J., Wang, X., An, Z., 2008. Millennial- and orbital-scale changes in the East Asia monsoon over the past 224,000 years. *Nature* 451, 1090–1093.

Waser, N.A.D., Harrison, P.J., Nielsen, B., Calvert, S.E., Turpin, D.H., 1998. Nitrogen isotope fractionation during the uptake and assimilation of nitrate, nitrite, ammonium, and urea by a marine diatom. *Limnology and Oceanography* 43, 215–224.

Weldeab, S., Lea, D.W., Schneider, R.R., Andersen, N., 2007. 155,000 years of West African monsoon and ocean thermal evolution: *Science* 316, 1303–1307.

https://doi.org/10.1017/qua.2020.118 Published online by Cambridge University Press